Ultrathin Dual-band Metamaterial Absorber

Huan Liu (20192850@neepu.edu.cn)
Northeast Electric Power University
Rui Wang
Northeast Electric Power University
Junyao Wang
Northeast Electric Power University
Tianhong Lang
Northeast Electric Power University
Bowen Cui
Northeast Electric Power University

Research Article

Keywords: metamaterial absorber, dual-band, ultrathin, polarization-insensitive

Posted Date: July 7th, 2021

DOI: https://doi.org/10.21203/rs.3.rs-663131/v1

Ultrathin dual-band metamaterial absorber

Huan Liu[1], Rui Wang[2], Junyao Wang[3], Tianhong Lang[4], Bowen Cui[5]*

Northeast Electric Power University

1 20192850@neepu.edu.cn; 2 2318956795@qq.com; 3 junyao_0001@126.com; 4 437337855@qq.com; 5 1024457201@qq.com

Abstract

In this paper, an ultrathin dual-band metamaterial absorber (MMA) is designed. Its top layer consists of two nested split-ring resonators. The calculation result demonstrates that there are two distinct absorption peaks, which are 9.258GHz and 21.336GHz, with absorption rate of 99.78% and 96.91%. It also show polarization-insensitive for normal incident and its thickness is only 1.96% of the wavelength of its lowest absorption frequency. Moreover, we explore the MMA's absorption mechanism and analyze the influence of main structural parameters on the MMA's absorption characteristics. The proposed MMA has simple structure and high absorption, it can be applied in electromagnetic stealth, bolometers, sensor and other fields.

Key word: metamaterial absorber, dual-band, ultrathin, polarization-insensitive

1. Introduction

The absorber based on metamaterial structure has become one of the research focuses because its electromagnetic parameters can be change by adjusting the structure's geometric parameters and shape to get impedance matching, so as to achieve perfect absorption. In 2008, Landy et al. [1] first designed a single-band MMA in microwave range, which achieved 88% absorption at 11.5GHz. Since then, researchers have designed many different types of MMAs, including single-band MMAs [2-4], multi-band MMAs [5-7], broadband MMAs [8-10] and tunable MMAs [11-13]. Its absorption frequencies have ranged from microwave, THz, infrared to visible light. In 2010, Tao H et al. designed and produced a dual-band MMA in the THz range [14], the experimental results showed that the MMA had both absorption peaks at 1.4THz and 3.0THz with absorption rate of 85% and 93%, respectively. In 2010, Li M et al. designed and produced a dual-band polarization insensitive MMA in the microwave range [15]. Simulation results showed that the two absorption peaks of the MMA were 11.5GHz and 16.01GHz with absorption rate of 97% and 99%, respectively. In 2012, Cheng H et al. designed and fabricated a polarization insensitive wide-angle dual-band MMA based on "#" shaped metal structure in the infrared range [16]. The MMA had two absorption peaks at the wavelength of 3.15μm and 5.86μm with absorption rate of 74% and 96%, respectively. In 2013, Ni B et al. also designed a dual-band polarization insensitive MMA [17], which had two absorption peaks at 10GHz and 20GHz with absorption rate of 96% and 99%, respectively. In 2016, Ayop O et al. designed a dual-frequency polarization-independent MMA based on two rings with different radius [18]. Simulation results showed that the MMA had two absorption peaks at 9GHz and 11GHz with absorption rate of 96.41% and 93.61%, respectively. MMAs have the advantages of thin thickness, small size, simple structure and high absorptivity, which can be widely used in electromagnetic stealth [19, 20], bolometers [21-23], sensor [24,25], solar photovoltaic [26,27] and other fields.

In this paper, a dual-band MMA is presented. Its top layer consists of two nested

split-ring resonators. And its absorption rate is very high, both absorption peaks' absorption rate are over 99%, and the thickness of the MMA is only 1.96% of the wavelength of its lowest absorption frequency. Then the polarization insensitivity and absorption mechanism of the MMA are discussed. Finally, the influence of main geometric parameters on the MMA's absorption characteristics are also analyzed.

2. Design and simulation

Structural unit schematic diagram of the designed dual-band MMA is illustrated in Fig.1. The MMA is composed of a classical three-layer structure: the top layer and bottom layer are metal, and the middle layer is dielectric. The top layer consists of two nested split-ring resonators, and the outer ring and inner ring are composed of a set of rectangular strips respectively. The top and bottom layer are copper, and its electric conductivity is σ=5.8×10^7*S*/m. The intermediate dielectric layer is FR-4, and its dielectric constant and the tangent of the loss angle are ε_r=4.3 and tanδ=0.025 respectively. The structural dimensions of the designed MMA is shown in Fig. 1(b). The periodic side length of the unit structure is *a*. The side length of the outer ring and the length and width of outer ring's rectangular strip are *b*, l_1 and w_1, respectively. The side length of the and the length and width of the inner ring's rectangular strip are *c*, l_2 and w_2, respectively. After repeated optimization, the optimized parameters value is shown in Table 1.

In this paper, CST Microwave Studio based on Finite Integration Technique (FIT) is adopted to study the absorption characteristics of the MMA. We use frequency domain solver and set x and y directions as unit cell and z directions as open (add space). Wave vector *k* is incident vertically along the z-axis, electric field *E* is in the -y direction, and magnetic field *H* is in the -x direction, as shown in Fig. 1(a). The absorption $A(\omega)$ can be expressed as:

$$A(\omega) = 1 - R(\omega) - T(\omega) \tag{1}$$

Where $R(\omega)$ and $T(\omega)$ are the reflectivity and transmission respectively, which can be calculated by formula $R(\omega) = |S_{11}|^2, T(\omega) = |S_{21}|^2$. When the underlying metal's thickness is much greater than the electromagnetic wave's skin depth in the metal, the transmission $T(\omega) = 0$. Reflectivity can also be expressed as:

$$R(\omega) = \frac{Z(\omega) - Z_0}{Z(\omega) + Z_0} \tag{2}$$

Where $Z(\omega) = \sqrt{\mu(\omega) / \varepsilon(\omega)}$ is material impedance, $Z_0 = \sqrt{\mu_0 / \varepsilon_0}$ is free space impedance. When the material impedance matches the free space impedance, the reflectivity $R(\omega) = 0$ .Therefore, when the underlying metal thickness is thick enough and the absorber achieves impedance matching, the absorber can achieve perfect absorption.

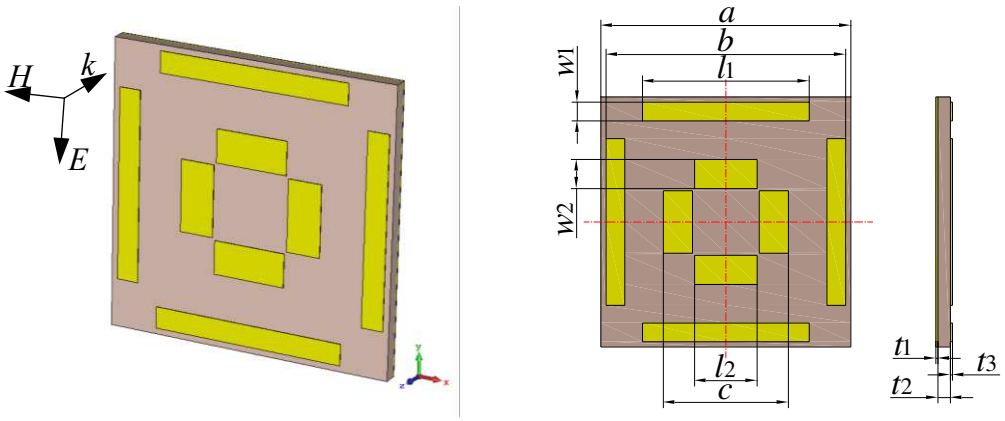

(a) (b)

Fig.1 Structure schematic of the dual-band MMA. (a) Three-dimensional view; (b) Top view and side view.

Table 1: Optimized parameter value.

a (mm)	b (mm)	c (mm)	t_1 (mm)	t_2 (mm)	t_3 (mm)	l_1 (mm)	l_2 (mm)	w_1 (mm)	w_2 (mm)
12.0	11.5	6.0	0.018	0.6	0.018	8.0	3.0	0.9	1.4

3. Result and discussion

The optimized absorption, reflection and transmission spectrum of the dual-band MMA is shown in Fig. 2. It indicate that there are two absorption peak, which are 99.78% at 9.258GHz and 99.91% at 21.336GHz. The absorption rate of the two absorption peaks is approximately 100%, and the thickness of the MMA is only 1.96% of the wavelength of its lowest absorption frequency.

Electromagnetic waves in nature contain different polarization components, so we investigate the polarization insensitivity of the dual-band MMA, as shown in Fig.3. The two absorption spectra almost completely coincide under the incident of TE and TM polarization waves, as shown in Fig. 3(a). The absorption spectrum curves are also almost coincident under the incident of different angles' polarization wave in TE mode, as shown in Fig. 3(b). Therefore, the designed MMA is polarization- insensitive.

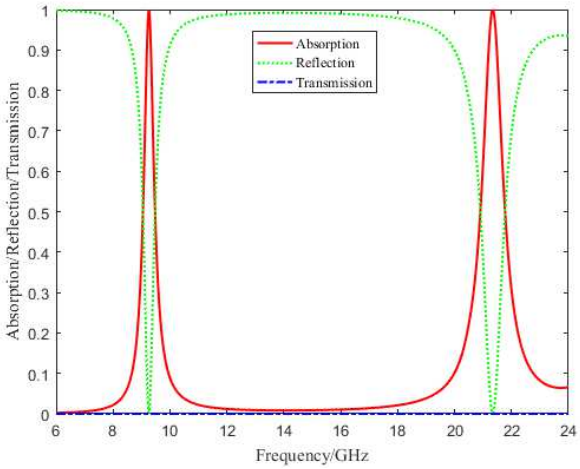

Fig.2 Simulated absorption, reflection and transmission spectrum of the dual-band MMA.

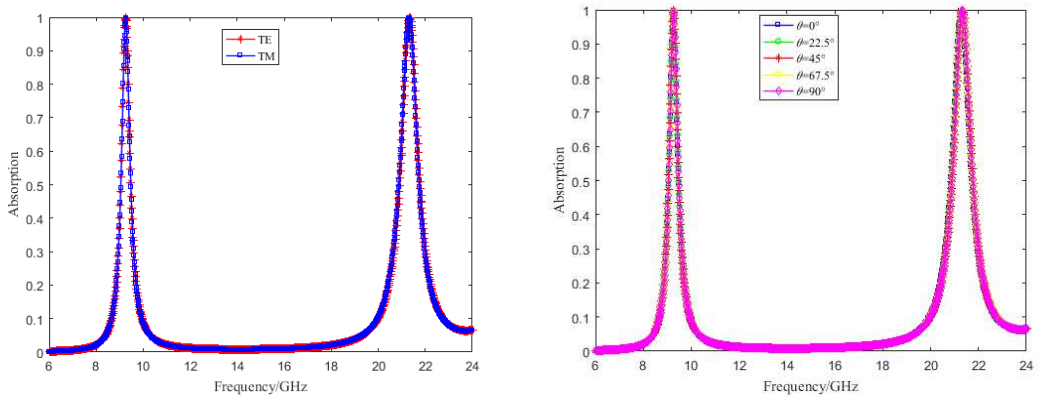

(a) (b)

Fig.3 (a) Simulated absorption spectra for TE and TM polarization wave; (b) Simulated absorption spectra for different polarization angle in TE mode.

In order to explore the MMA's absorption mechanism, the electric field, surface current distribution and magnetic field distribution of the MMA under normal incident electromagnetic wave is calculated, as shown in Fig.4, Fig.5 and Fig.6. When the frequency of the incident electromagnetic wave is 9.258GHz, the electric field, magnetic field and surface current of the dual-band MMA are mainly distributed in the region of the outer ring. When the frequency of the incident electromagnetic wave is 21.336Hz, the electric field, magnetic field and surface current of the dual-band MMA are mainly distributed in the region of the inner ring. That is because under the action of electric field component of electromagnetic wave, positive and negative charges in the rectangular strip gather to both ends respectively and generate strong electric field, as shown in Fig. 4(a) and Fig. 4(c). The charge in the metal strip is induced to the bottom metal layer, causing the bottom metal to generate opposite charge accumulation, thus forming an opposite electric field distribution in the bottom metal, as shown in Fig. 4(b) and Fig. 4(d). The accumulation of opposing charges in the metal layer creates an electric dipole that causes an electric resonance in the metal layer. Due to the reverse charge distribution in the upper and lower metal layers, the reverse current distribution in the upper and lower metal layers is formed, as shown in Fig. 5. The reverse currents in the upper and lower metal layers indicates the occurrence of magnetic resonance in the absorber, and the magnetic field distribution is obtained as shown in Fig. 6. Under the action of electric resonance and magnetic resonance, the metamaterial absorber consumes the energy of the electromagnetic wave incident to the absorber, thus generating the absorption peaks. Through calculation, the power loss curve of the absorber is obtained, as shown in Fig.7. It can be seen that the energy absorbed by the absorber is mainly consumed in the dielectric layer through magnetic resonance.

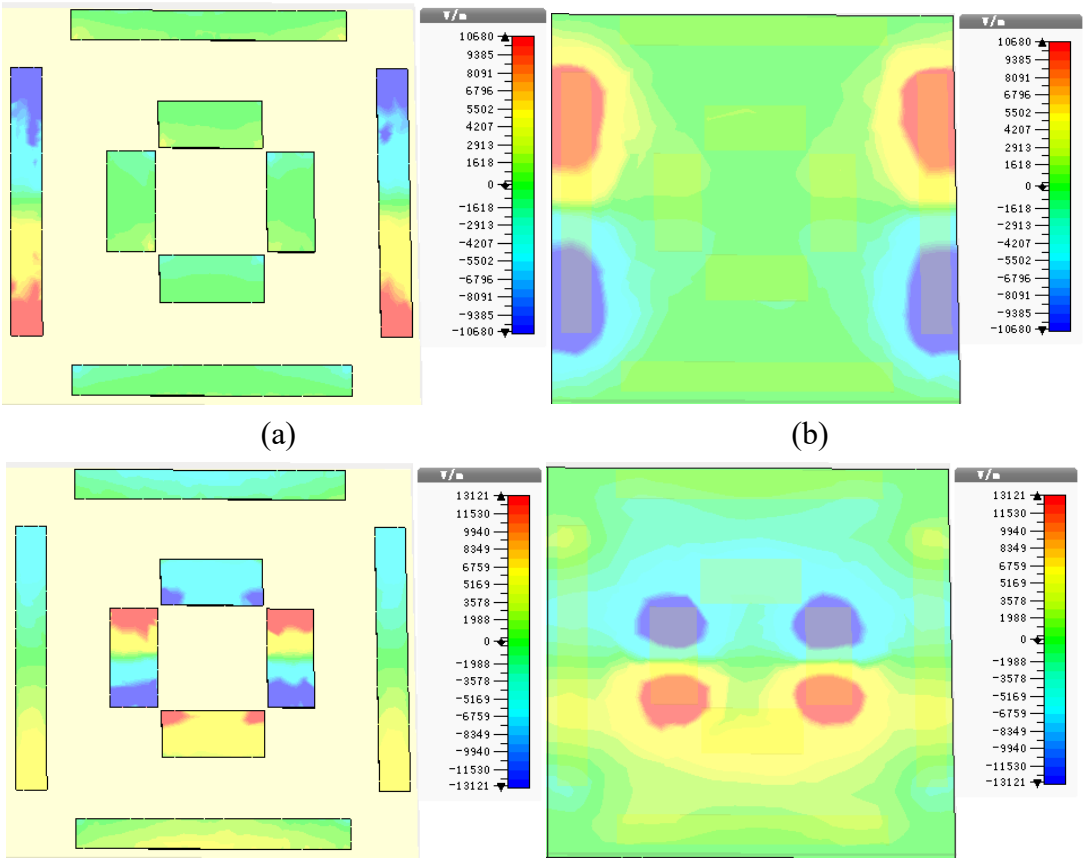

(a) (b)

(c) (d)

Fig.4 Electric field [real (E_z)] distribution of the dual-band MMA. (a) Top layer at 9.258GHz; (b) Bottom layer at 9.258GHz; (c) Top layer at 21.336GHz; (d) Bottom layer at 21.336GHz.

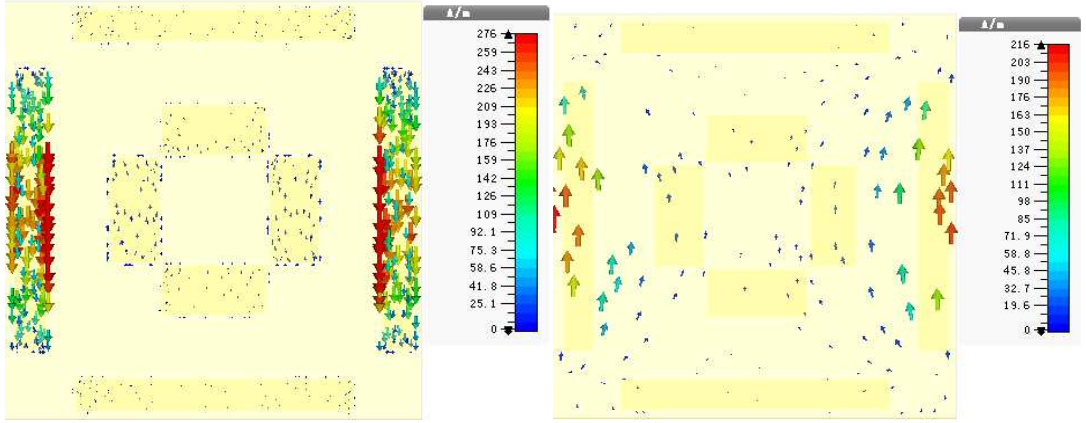

(a) (b)

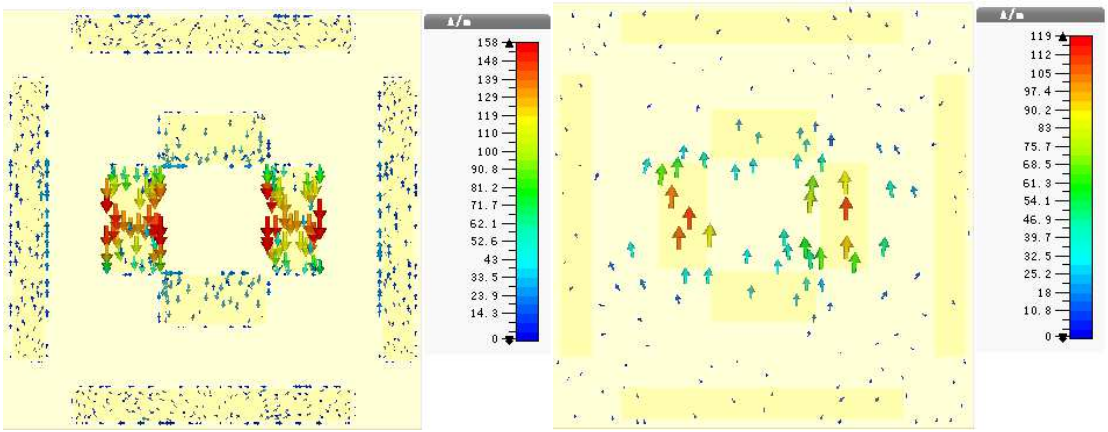

(c) (d)

Fig.5 The surface current [real (*I*)] distribution of the dual-band MMA. (a) Top layer at 9.258GHz; (b) Bottom layer at 9.258GHz; (c) Top layer at 21.336GHz; (d) Bottom layer at 21.336GHz.

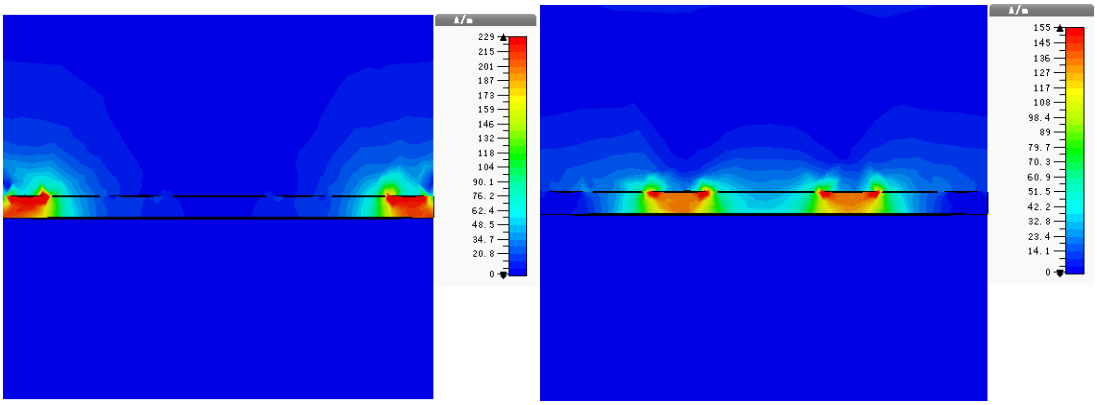

(a) (b)

Fig. 6 The Magnetic field [abs (*H*)] distributions of the designed dual-band MMA in the *x*-*z* plane (*y*=0). (a) 9.258GHz; (b) 21.366GHz.

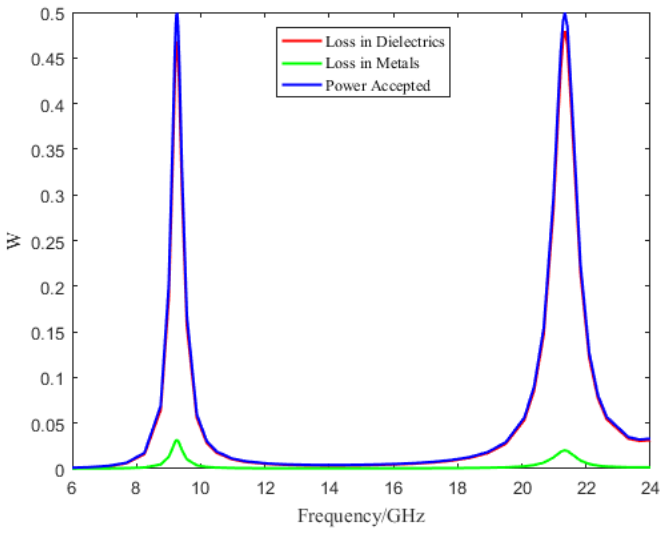

Fig. 7 Power loss in the dual-band MMA.

In addition, the influence of main geometric parameters on the MMA's absorption characteristics are also analyzed, as shown in Fig.8. When the length of the rectangular strip of the outer ring l_1 increases from 6.5mm to 8.5mm with a step length of 0.5mm, the absorption rates of the two absorption peaks almost remain unchanged. The absorption frequency of the low frequency peak gradually shifts from 11.112GHz to 8.799GHz, and the absorption frequency of the high frequency peak varies in 21.282GHz-21.444GHz. When the rectangular strip of the inner ring l_2 increases from 2.7mm to 3.1mm with a step length of 0.1mm, both absorption peaks have a red shift. The absorption frequency of the low frequency peak moves from 9.312GHz to 9.258GHz, and that of the high frequency peak moves from 23.154GHz to 20.922GHz. With the increase of l_2, the absorption rate of the low frequency peak is basically unchanged, while the absorption rate of the high frequency peak gradually increases from 93.22% to 99.99%. When the intermediate dielectric layer thickness of the absorber t_2 increases from 0.4mm to 0.8mm with a step length of 0.1mm, the absorption frequency of the low-frequency absorption peak varies in 9.258GHz-9.1837GHz, and its absorption rate first increases and then decreases and reaches the maximum at t_2 =0.6mm. With the increase of t_2, the absorption frequency of the high frequency absorption peak gradually shifts from 22.524GHz to 20.634GHz, and its absorption rate firstly increases and then decreases and reaches the maximum at t_2=0.7mm. According to the above analysis, the low frequency absorption peak is mainly affected by the rectangular strip of the outer ring, while the high frequency absorption peak is mainly affected by the rectangular strip of the inner ring. The magnetic resonance mainly occurs in the dielectric layer, so the thickness of the dielectric layer t_2 has an effect on both absorption peaks.

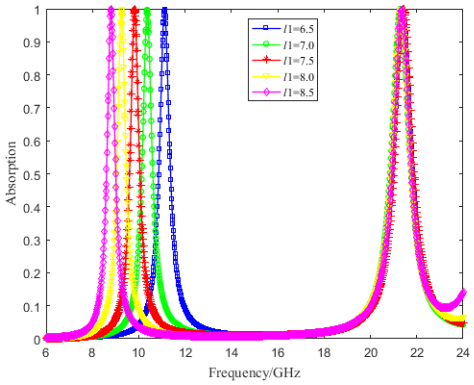

(a)

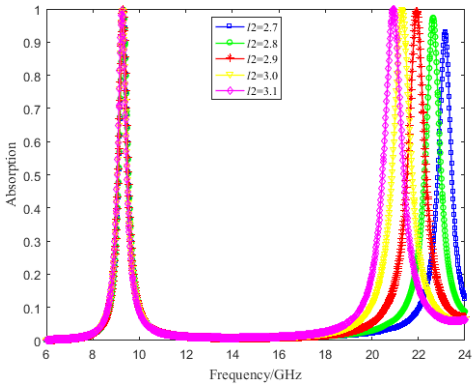

(b)

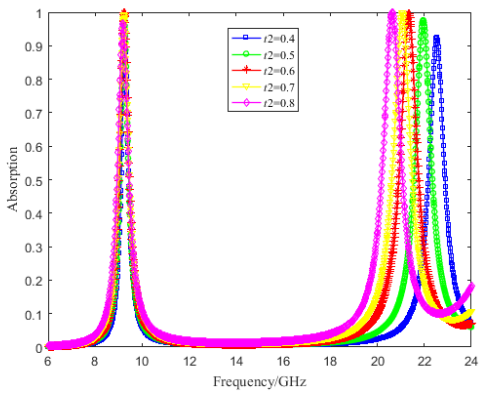

(c)

Fig. 8 Influence of different parameter values on the absorption with other parameters fixed. (a) Parameter l_1; (b) Parameter l_2; (c) Parameter t_2

4. Conclusion

In this paper, an ultrathin dual-band MMA is designed, and its top layer consists of two nested split-ring resonators. The simulation show that there are two distinct absorption peaks, which are 9.258GHz and 21.336GHz, with absorption rate of 99.78% and 96.91%. It also show polarization-insensitive for normal incident and its thickness is only 1.96% of the wavelength of its lowest absorption frequency. The main structure parameters affect the dual-band MMA's absorption are analyzed. Parameter l_1 mainly affects the low frequency absorption peak, parameter l_2 mainly affects the high frequency absorption peak, and parameter t_2 has a great influence on both absorption peaks. Because the MMA has simple structure and high absorption, it can be widely applied in electromagnetic stealth, bolometers, sensor and other fields.

Reference

[1] Landy N I, Sajuyigbe S, Mock J J, et al. Perfect metamaterial absorber[J]. Physical review letters, 2008, 100(20): 207402.

[2] Tao H, Landy N I, Bingham C M, et al. A metamaterial absorber for the terahertz regime: design, fabrication and characterization.[J]. Optics Express, 2008, 16(10):7181-7188.

[3] Liu X, Starr T, Starr A F, et al. Infrared spatial and frequency selective metamaterial with near-unity absorbance[J]. Physical review letters, 2010, 104(20): 207403.

[4] Guo L, Ma X, Zou Y, et al. Wide-angle infrared metamaterial absorber with near-unity absorbance[J]. Optics & Laser Technology, 2018, 98:247-251.

[5] Wen Q Y, Zhang H W, Xie Y S, et al. Dual band terahertz metamaterial absorber: Design, fabrication, and characterization[J]. Applied Physics Letters, 2009, 95(24): 241111.

[6] Rufangura P, Sabah C. Dual-band perfect metamaterial absorber for solar cell applications[J]. Vacuum, 2015, 120(Part B):68-74.

[7] Meng T, Hu D, Zhu Q. Design of a five-band terahertz perfect metamaterial absorber using two resonators[J]. Optics Communications, 2018, 415:151-155.

[8] He S, Jin Y, Ye Y Q. Omnidirectional, polarization-insensitive and broadband thin absorber in the terahertz regime[J]. Josa B, 2010, 27(3):498-504.

[9] Ma W, Wen Y, Yu X. Broadband metamaterial absorber at mid-infrared using multiplexed cross resonators[J]. Optics Express, 2013, 21(25):30724-30730.

[10] Kang Y, Liu H. Wideband absorption in one dimensional photonic crystal with graphene-based hyperbolic metamaterials[J]. Superlattices & Microstructures, 2017.

[11] Zhu B, Feng Y, Zhao J, et al. Switchable metamaterial reflector/absorber for different polarized electromagnetic waves[J]. Applied Physics Letters, 2010, 97(5):051906 - 051906-3.

[12] Wang B X, Wang L L, Wang G Z, et al. Frequency Continuous Tunable Terahertz Metamaterial Absorber[J]. Journal of Lightwave Technology, 2014, 32(6):1183-1189.

[13] Zhou Q, Liu P, Bian L A, et al. Controlling enhanced absorption in graphene metamaterial[J]. Optics Communications, 2018, 413:310–316.

[14] Tao H, Bingham C M, Pilon D, et al. A dual band terahertz metamaterial absorber[J]. Journal of Physics D Applied Physics, 2010, 43(22):225102.

[15] Li M, Yang H L, Hou X W, et al. Perfect Metamaterial Absorber with Dual Bands[J]. Progress in Electromagnetics Research, 2010, 108(4):37-49.

[16] Cheng H, Chen S, Yang H, et al. A polarization insensitive and wide-angle dual-band nearly perfect absorber in the infrared regime[J]. Journal of Optics, 2012, 14(8):85102-85106(5).

[17] Ni B, Chen X S, Huang L J, et al. A dual-band polarization insensitive metamaterial absorber with split ring resonator[J]. Optical & Quantum Electronics, 2013, 45(7):747-753.

[18] Ayop O, Rahim M K A, Murad N A, et al. Dual-resonant polarization-independent and wide-angle metamaterial absorber in X-band frequency[J]. Applied Physics A,

2016, 122(4):374.
[19] Iwaszczuk K, Strikwerda A C, Fan K, et al. Flexible metamaterial absorbers for stealth applications at terahertz frequencies [J]. Optics Express, 2012, 20(1):635-643
[20] Wang B Y, Liu S B, Bian B R, et al. A novel ultrathin and broadband microwave metamaterial absorber[J]. Journal of Applied Physics, 2014, 116(9):207402-4058.
[21] Xu C, Qu S, Pang Y, et al. Metamaterial absorber for frequency selective thermal radiation[J]. Infrared Physics & Technology, 2017, 88.
[22] Niesler F B P, Gansel J K, Fischbach S, et al. Metamaterial metal-based bolometers[J]. Applied Physics Letters, 2012, 100(20): 203508.
[23] Zhou Y, Feng T, Liang Z, et al. An ultra-thin isotropic metamaterial thermal radiator[J]. EPL (Europhysics Letters), 2011, 96(2): 24005.
[24] Karaaslan M, Ünal E, Akgöl O, et al. Microwave metamaterial absorber for sensing applications[J]. Opto-Electronics Review, 2017, 25(4).
[25] Chen C, Sheng Y, Wang J. Computed a multiple band metamaterial absorber and its application based on the figure of merit value [J]. Optics Communications, 2017, 406.
[26] Wan C , Ho Y , Nunez-Sanchez S , et al. A Selective Metasurface Absorber with An Amorphous Carbon Interlayer for Solar Thermal Applications [J]. Nano Energy, 2016:S2211285516301355.
[27] Lin K, Chen H, Lai Y, et al. Loading effect–induced broadband perfect absorber based on single-layer structured metal film[J]. Nano Energy, 2017, 37.